PCCP

Accepted Manuscript

ROYAL SOCIETY OF CHEMISTRY

www.rsc.org/pccp

Proton triggered emission and selective sensing of picric acid by the fluorescent aggregates of 6,7-dimethyl-2,3-bis-(2-pyridyl)-quinoxaline

Prativa Mazumdar[†], Samir Maity[†], Milan Shyamal[†], Debasish Das[†], Gobinda Prasad Sahoo[†] and Ajay Misra[†]

[†]*Department of Chemistry and Chemical Technology, Vidyasagar University, Midnapore 721 102, W.B, India*

Abstract:

A heteroatom containing organic fluorophore 6,7-dimethyl-2,3-bis-(2-pyridyl)-quinoxaline (BPQ) is weakly emissive in solution but its emission property is highly enhanced in the aggregated state due to restriction of intramolecular rotation (RIR) and large amplitude vibrational modes, demonstrating the phenomena, aggregation induced emission enhancement (AIEE). It has strong proton capture capability, allowing reversible fluorescence switching in basic and acidic medium and the emission color changes from blue to green in aggregated state through protonation. It has been explained as competition between intramolecular charge transfers (ICT) and the AIEE phenomena at lower pH range (pH~1-4). Such behavior enables it as a fluorescent pH sensor for detecting acidic and basic medium. Morphologies of the particles are characterized using optical and field emission scanning electron microscopic (FESEM) study. The turn off fluorescence property of aggregated BPQ has been utilized for selective detection of picric acid and the fluorescence quenching is explained due to ground state complexation with strong quenching constant, 7.81×10^4 M^{-1}.

1. Introduction:

Luminescent materials have received a great deal of attention because of their potential applications in chemistry, materials science and biology.[1-4] The fluorescence (FL) based technique offers high sensitivity, low background noise and wide dynamic ranges.[5,6] Development of efficient luminescent materials makes them ideal candidates for high-tech applications in solid state such as organic light emitting diode (OLED),[7-9] organic photovoltaic (OPV),[10,11] organic field effect transistor (OFET),[12,13] sensors[14-17] etc. Scientists are in perpetual quest for luminescent materials that can emit efficiently in the solid state as for most of the real-world applications require the luminophores as solid films. Most organic fluorophores contain planar π-conjugated aromatic rings, which may increase the chances for molecular aggregation to form excimers and exciplexes.[18,19] Such molecular aggregation will cause the fluorescence quenching of fluorophores in the solid state or in concentrated solutions due to the nonradiative deactivation of the excited state, which is known as aggregation-caused quenching (ACQ). Normally, ACQ greatly limits the applications of the aromatic hydrocarbon fluorophores and their derivatives for light-emitting materials and devices in the aggregated state. Thus, there is a high demand for the development of simple, stable FL sensors.

In 2001 Tang[20] and Park[21] first reported a class of interesting tetraphenylsiloles derivatives that were nonemissive in dilute solutions but exhibited intense emission in concentrated solutions or in the solid state. This unique phenomenon is called "Aggregation-induced emission" (AIE)[22] effect. A variety of luminogenic molecules can exhibit this effect but the most common feature of this entire AIE active molecule is that they contain multi aromatic ring with free rotating parts.[23-30] They are classified in two different groups. In the first group, non emissive molecule become emissive in its solid state and is exactly opposite to the ACQ effect. As the emission is induced due to aggregation, this effect is known as "Aggregation-induced emission" (AIE).[22] In the second group, weakly emissive molecules become strongly emissive in their aggregated state and this effect is termed as "Aggregation induced emission enhancement" (AIEE).[31]

This unique characteristic differentiates them from conventional luminophores and focused on the exploration of their utilities in the development of optical sensors and other important applications. Functional chromophore containing embedded recognition elements showing shifts in both absorption and emission upon acid/base stimuli are of immense interest for their innately potential applications in sensors.[32-37] Great effort has been devoted to the molecular design, modification[38-41] and origin of the spectral shift upon protonation of functional chromophores but in most investigations the spectral shift in presence of acid stimuli shows hypsochromic shift due to protonation. Since lone pairs of heteroatom lose conjugation, this hypsochromism in spectra is an obvious incident.[42] But proton triggered bathochromic shift is very rare.

Materials using non-covalent interactions *e.g.* hydrogen bonding and π-stacking, is being continuously explored in the field of sensing chemistry.[43-45] Depending on the nature of the interaction and the constituents involved, this selectivity can then be used in a wide variety of chemo-sensing processes.[46] Due to high selectivity and sensitivity, fluorescent chemo-sensors have found potential applications in the detection of environmentally important analytes such as nitroaromatic (NA) explosives.[46] Most commonly this fluorescence sensing is occurred by photoinduced electron transfer (PET) mechanism that depends on the excited state energy gap between the fluorophore and the quencher, and binding efficiency of the fluorophore and the quencher molecules also.[47] Nitroaromatic compounds are electron deficient and they prefer to form aromatic π-interactions complexes with the electron-rich aromatic host.[48] The presence of nitro groups can further enhance the complexation through hydrogen bonds with suitable donor groups on the host molecules. Among the different nitroaromatic compounds, picric acid (PA) is one of the powerful explosive. PA is also a non-biodegradable environmental pollutant, which causes several problems to human health, such as skin irritation, skin allergy, cancer and respiratory system and liver damage.[49] Large quantities of PA are used in the pharmaceutical, dye and firework industries as a chemical reagent and released into the environment, which eventually enters the food chain.[50] Thus the development of a fast and selective method for the detection of PA is highly

desirable. In the past few years, different types of effective fluorescent sensors emerged for PA. Although the first selective sensor for PA was reported in 2004, this field needs to be explored further for suitable sensors.[51] In 2012, intermolecular charge transfer (ICT) based probes were reported by Kumar *et al.*[52] However, many of the previously reported sensors had several drawbacks which include low binding affinity to PA and interference from other nitro compounds. Most of PA sensor systems were studied in molecular state. Further the lack of stability of organic fluorophore in water limit the detection of water soluble nitro-aromatic. But the fluorescent aggregated hydrosol has this advantage over other organic sensors.

Here we report a low dimensional material from 6,7-dimethyl-2,3-bis-(2-pyridyl)-quinoxaline (BPQ) where two free twisting pyridyl rings, attached to the 2 and 3 position of 6,7-dimethyl quinoxaline moiety are seized in solid phase by restriction of intramolecular free rotation (Scheme 1). It exhibits strong AIEE effect and is manifested by changing the colorless solution to blue color in aggregate state under UV irradiation. Another interesting part of BPQ hydrosol is its proton triggered tunable aggregation induced emission enhancement (AIEE) and intramolecular charge transfer (ICT) property. In presence of proton, an unusual bathochromic shift is observed in both absorption and emission spectra and the color of hydrosol changes from blue to green. The pH triggered bathochromic shift in emission has been explained due to introduction of charge transfer character in BPQ upon protonation to its pyridyl group. This aggregated BPQ hydrosol is utilized in sensing picric acid which is a powerful explosive among the different nitroaromatic compounds. It can selectively sense PA by forming ground state complexation with PA in its aggregated state.

Scheme 1: Chemical structure of BPQ

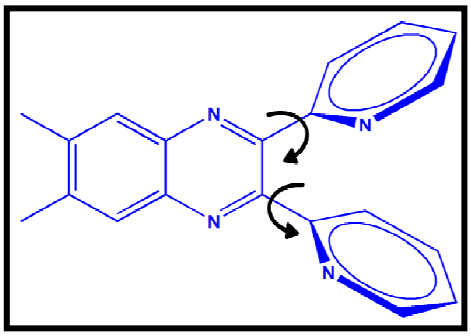

2. Experimental:

Materials: 6,7-dimethyl-2,3-bis-(2-pyridyl)-quinoxaline(BPQ) was purchased from Sigma-Aldrich Chemical Corp. Tetrahydrofuran (THF), Hydrochloric acid (HCl), Sodium hydroxide (NaOH), picric acid (PA), dinitro benzene (DNB), 4-nitrophenol (NP), 2,4-dinitrophenol (DNP), 3,5-dinitrobenzoic acid(3,5-DNBA), 3-nitrobenzoic acid(3-NBA), 4-nitroaniline (NA) and 2,4-dinitro toluene (DNT) were purchased from E-Merck India Ltd. The purity of these chemicals was checked spectrophotometrically. Triply distilled deionised water was used throughout the experiment.

Preparation of aggregates: 0.02(M) solution of BPQ was prepared using THF as good solvent. Different amount of the above solution (10μL for Sample A, 20μL for Sample B, 30μL for Sample C, 100μL for Sample D) were injected drop wise into 1:9 (v/v) ratio of THF/water and allowed to stir for 2 min. The final concentrations of BPQ were 40μM, 80μM, 120μM, 400μM for sample A,B,C,D respectively. Clearness of the solutions was gradually decreased and a milky white color was appeared. Then the solutions were allowed to stand for 20 min.

For pH variation study, pH of the medium was adjusted by adding different amount of 0.1(M) HCl and 0.1(M) NaOH and the subsequent measurement of pH by using a pH meter. All solutions were prepared on the same day to study their absorbance, steady-state and time-resolved fluorescence measurements.

Characterization: The UV-Vis spectroscopy was used to characterize the optical properties and was measured in a 1cm quartz cuvette with a Shimadzu UV-2450 spectrophotometer. The spectra were recorded at room temperature in the range between 230 nm to 450 nm. Steady state fluorescence spectra were recorded using Hitachi F-7000 Fluorescence Spectrophotometer. Time-resolved fluorescence measurements were carried out under ambient conditions using a time-correlated single-photon counting (TCSPC) spectrometer [a picosecond diode laser (IBH, UK)] all samples were excited using 376 nm picosecond diode laser and the emission were collected at 398 nm and 468 nm depending upon the nature

of emission of the sample. Lamp profiles were measured with a band-pass of 3 nm using Ludox as the scatterer. The decay parameters were recovered using a non-linear iterative fitting procedure based on the Marquardt algorithm.[53] The quality of fit was assessed over the entire decay, including the rising edge, and tested with a plot of weighted residuals and other statistical parameters *e.g.* the reduced χ^2 ratio.[54] All pH measurements were made with an ORION VERSASTAR. The morphologies of the synthesized nano/micro structures were studied using ZEISS EVO 18 scanning electron microscope (SEM) operated at an accelerating voltage of 5 kV. Before SEM study samples were vacuum dries on a glass plate and a thin layer of Au was deposited onto the samples to minimize sample charging. Optical microscopy images were taken using an NIKON ECLIPSE LV100POL upright microscope equipped with a 12V-50W mercury lamp. The samples for optical microscopic study were prepared by placing a drop of colloidal solution onto a clean glass slide. All the experiments were carried out at room temperature.

Computational Method: Ground state geometry of BPQ was optimized by Density Functional Theory (DFT) based computation using hybrid functional (B3LYP) with 6-31G(d,p) basis set. Excited state optimization of the protonated and neutral structures of BPQ were carried out by TDDFT based computation with 6-31G(d,p) basis set. HOMO, LUMO energy gap and electronic charge distribution of BPQ were computed using DFT based computation with hybrid functional (B3LYP) and 6-31G(d,p) basis set. All the computations on BPQ in this present study were carried out using Gaussian-09 software package program.

3. Results and Discussion:

UV-Vis Absorption Properties: Fig.1a outlines the absorption spectra of 80μM BPQ in THF. There are two distinct absorption bands in the UV-Vis spectra of BPQ. The band in the region 230 nm-280 nm is structured one and 310 nm-380 nm band is broad and structureless. The high energy structure band is the $S_0 \rightarrow S_1$ transition of the quinoxaline group and the broad structureless band which is solvent polarity sensitive is the charge transfer band arises due to charge transfer from pyridyl groups attached at 2 and 3

positions to quinoxaline. A clear bathochromic shift of the broad band is observed (fig.1a) as the polarity of the medium is increased from cyclohexane (ε=2.02) to THF (ε= 7.5) to DMSO (ε=48). But the structure band is insensitive towards solvent polarity except the relative change of intensities of the vibronic bands. UV-Vis absorption spectra of the stock solution (80μM BPQ in THF) and the aggregated hydrosol (different concentration of BPQ in THF was added to a fixed volume fraction of water) are shown in fig.1b. Though spectral position of hydrosol remain in the same position as that of the stock solution, the intensity of absorption band increases with the increasing concentration of BPQ in the hydrosol. Charge transfer state of BPQ in the aggregates behaves like Frankel exciton and is more stable than the charge transfer state of free molecule. This is reflected in the increased absorption of CT band of hydrosol than the free BPQ in good solvent having same BPQ concentration (sample B) (fig.1b). Increasing absorbance of hydrosol with increasing BPQ concentration is due to increased number of excitonic state within the aggregates. UV-Vis absorption spectra of hydrosol for a fixed BPQ concentration and increasing volume percentage of water are shown in fig.1c. It is observed that the absorption intensity of hydrosol increases with slight red shift of the CT band, with the increasing volume percentage of water in the solvent mixture.

The increasing number of particles with increasing water volume percentage is responsible for increased absorption of excitonic state and the bathochromic shift of spectra is due to enhanced dielectric constant of the medium. A closer look of CT band (fig.1a) illustrates its asymmetric nature *i.e.* the band is the superposition of two Gaussian peaks with maxima at 339 nm and 352 nm. The dipoles of two pyridyl rings are present in oblique orientation. Now the interaction energy between two identical chromophores with one in an excited electronic state may be given by this general form.

$$E_{interaction} = \Delta E \pm E_{resonance} \qquad \text{..... (i)}$$

Where ΔE contains electrostatic polarization and dispersion contribution and $E_{resonance}$ is the resonance interactions between two pyridyl groups (Scheme 2). This effectively split the excited state charge

transfer surface into two states. The $E_{resonance}$ can be calculated from the spectral splitting lines $\bar{\upsilon}$ and $\bar{\upsilon}'$ and it is found to be 2840cm^{-1}.

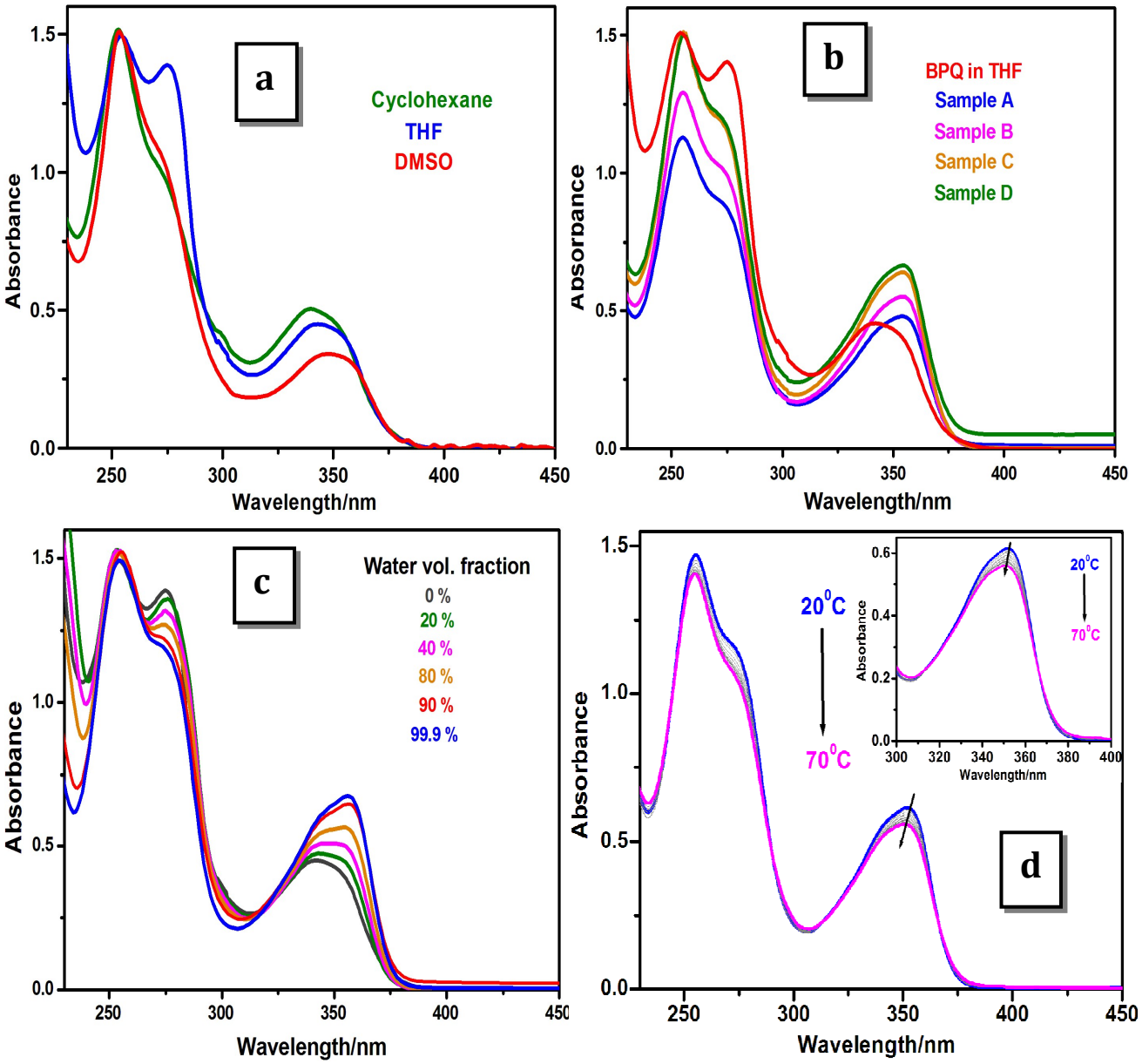

Fig.1 (a) UV-Vis absorption spectra of 80µM BPQ in (i) Cyclohexane, (ii) THF and (iii) DMSO. (b) UV-Vis absorption spectra of (i) 80µM BPQ in THF, (ii) sample A (40µM BPQ), (iii) sample B (80µM BPQ), (iv) sample C (120µM BPQ) and (v) sample D (400µM BPQ). (c) UV-Vis absorption spectra of 80µM BPQ in (i) 0% water (BPQ in THF), (ii) 20% water, (iii) 40 % water, (iv) 80 % water, (v) 90% water and

(vi) 99.9% water. (d) Variable temperature absorption spectra of aggregated BPQ in THF/water mixture (10:90 v/v). BPQ concentration: 80μM.

Scheme 2. Energy level diagram

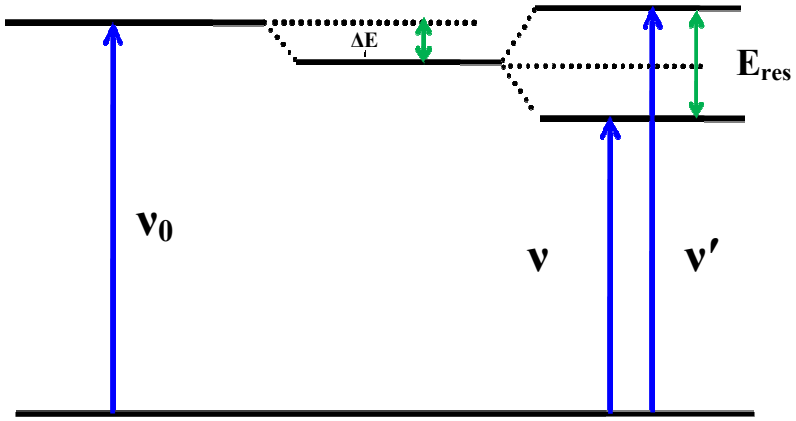

Temperature variation absorption study of aggregated BPQ (sample B) is shown in fig.1d. Fig.1d illustrates a small blue shift from 352 nm to 349 nm and coalescence of the asymmetric CT band as the temperature is increased from 20^0C to 70^0C. The increasing temperature causes crystal softening which results less favor charge transfer orientation of quinoxaline and pyridyl groups. On the other hand, two pyridyl groups take less favored orientations for mutual interaction which leads to coalescence of the spitted band with increasing temperature.

Photoluminescence study: The primary way to test whether a compound is AIEE active or not is to make a comparison of the emission spectra between its aggregated and molecular state. Since THF is a good solvent for BPQ and water is a poor one, aggregation of BPQ takes place with the increasing volume fraction of water in the solution. It is observed that the fluorescence of BPQ is gradually intensified when water is progressively added into its THF solution (Fig.2a). As the volume fraction of water (f_w) reaches 90%, the luminogenic molecules are aggregated into particles and emit intense blue light with emission maximum at 398 nm. The PL intensity is increased about 475 times at f_w = 90% compare to f_w = 0% at same BPQ concentration (80μM) under identical measurement conditions,

indicating the excellent AIEE property of BPQ (Fig.2b). Rotations and large amplitude vibrations of pyridyl groups (scheme 1) effectively deactivate the excited BPQ in good solvent through non radiative process and making it non-emissive. On the other hand, restriction of the intramolecular rotations and large amplitude vibrations of pyridyl groups of BPQ in the aggregates block the channel of nonradiative decay and make the molecule a strong emitter. A decrease in the PL intensity of BPQ hydrosol with a blue shift in emission peak from 398 nm to 396 nm is observed when the water fraction is increased from 90% to 99.9% (fig.2b). This is due to the possible formation of amorphous agglomerate with random stacking structures. In mixed solvent (THF-water) with low water content, the BPQ molecules steadily assemble in an ordered fashion to form more emissive, crystalline aggregates. But in higher water content, BPQ molecules may quickly agglomerate in a random fashion to introduce crystal softening within the crystalline aggregates. The change of emission color from colorless to intense blue in presence of 0% and 90% water content under UV irradiation is shown in the inset of fig.2b.

We also followed the time course of spectral evolution of BPQ hydrosol in 90% volume percentage of water (fig.2c). PL intensity increases with time and reaches the maximum intensity after 20 min of its preparation. Initially the mechanical shear stress leads to the increasing chances of most probable collisions; thus a portion of BPQ molecules clustered together to form tiny particles. The remaining portion of BPQ molecules present in the solvent mixture then gradually deposited onto the initially formed particle in recrystallization pattern to give highly emissive aggregated structures. The system thus attains an ordered cluster which restricts the free rotation and large amplitude vibrations of BPQ with time and the enhanced emission from the aggregated hydrosol is observed.

Optimum concentration of BPQ for PL study is achieved by adding different volume of 20mM BPQ in THF-water mixture (10:90 v/v). It has been observed that the PL intensity increases with increasing concentration of BPQ reaches a maximum at 80μM and then decreases with further increase in BPQ concentration (fig.2d). This suggests that 80μM is the optimum concentration of BPQ in solution below which aggregation of BPQ occurs in such a way that it can form emissive crystalline structure but

with further increase (>80 μM) in concentration BPQ orient in random fashion to soften the microcrystals and is responsible for decreasing emission intensity from hydrosol.

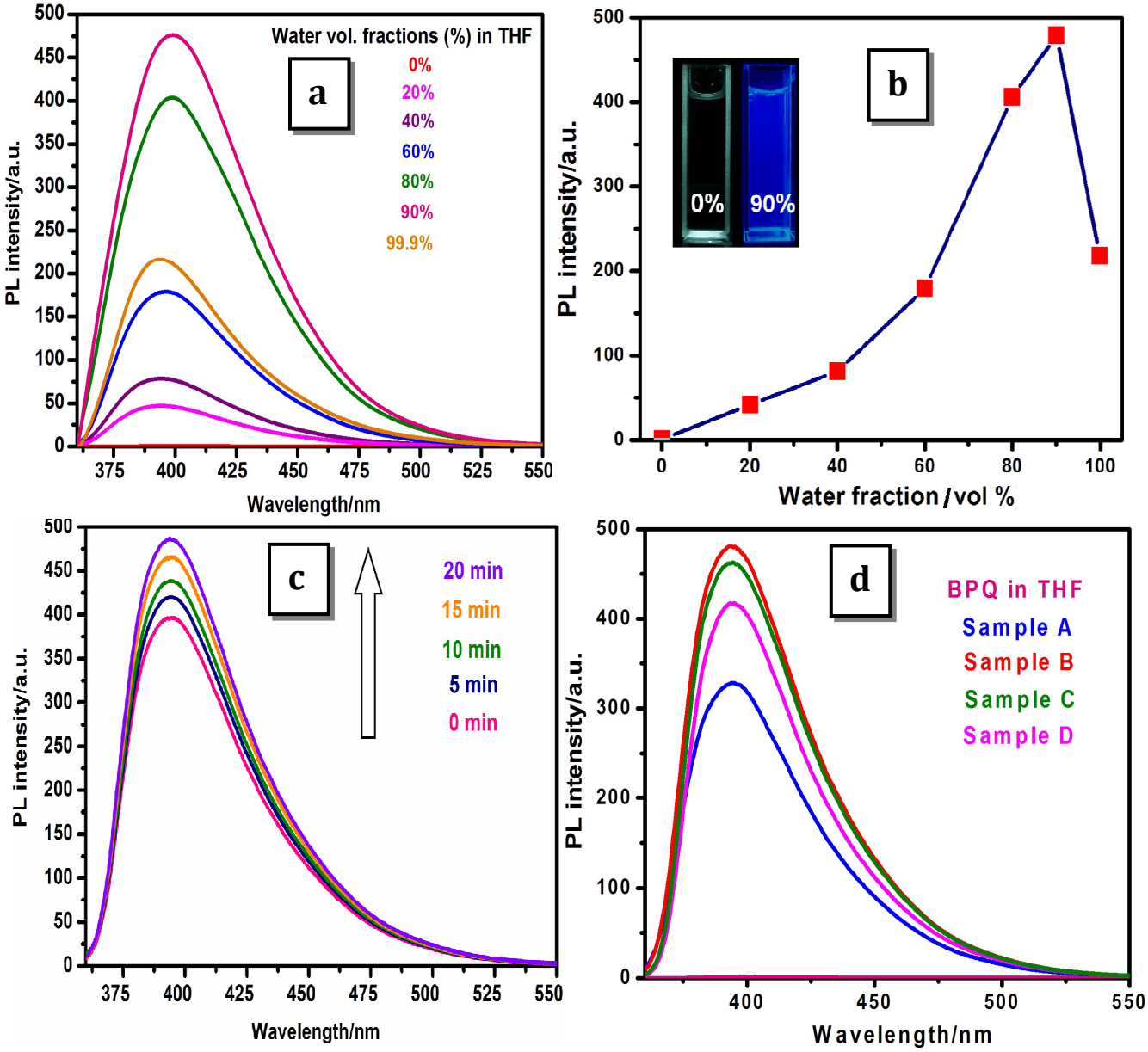

Fig.2 (a) Emission spectra of freshly prepared BPQ (80μM) in (i) 0% water (BPQ in THF), (ii) 20% water, (iii) 40% water, (iv) 60% water, (v) 80% water, (vi) 90% water and (vi) 99.9% water. λ_{ex}: 350 nm. (b) Plot of relative variation of PL intensity against water content (f_w) in THF/water mixture. BPQ concentration: 80μM. λ_{ex}: 350 nm. Insets: Fluorescence images of BPQ (0% and 90% H_2O) under 367 nm

illumination. (c) Dependence of the PL intensity of BPQ immediate after its preparation with time in THF/water mixture (10:90 v/v). BPQ concentration: 80μM. λ_{ex}: 350 nm. (d) Emission spectra of (i) 80μM BPQ in THF, (ii) sample A (40μM BPQ), (iii) sample B (80μM BPQ), (iv) sample C (120μM BPQ) and (v) sample D (400μM BPQ) in THF/water mixture (10:90 v/v).λ_{ex}: 350 nm.

FE-SEM Study:

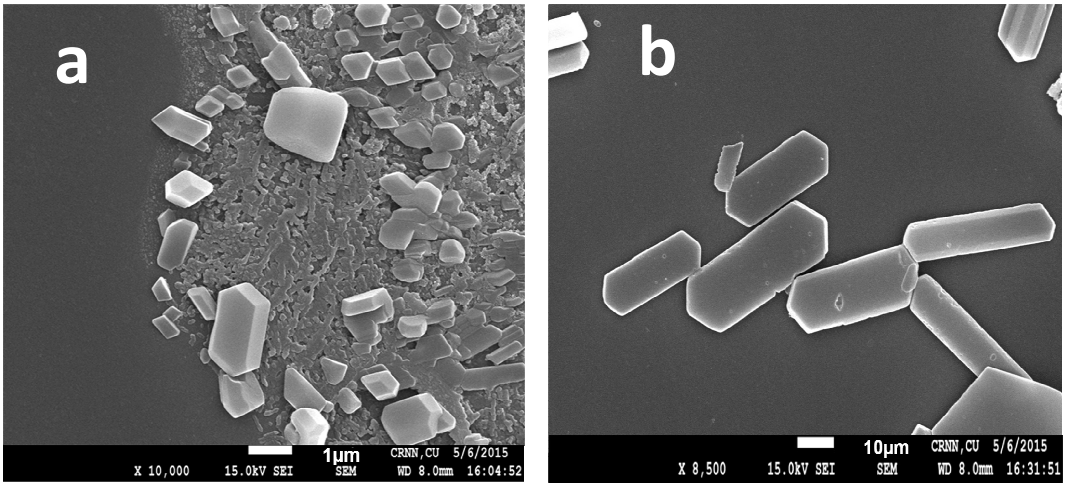

Fig.3 FESEM images of BPQ microstructures at concentration (a) sample C (120μM BPQ) and (b) sample D (400μM BPQ).

Field emission scanning electron microscopic (FESEM) study was carried out to study the morphology of the aggregated BPQ in the hydrosol. At low BPQ concentration, small crystalline microparticles (sample C) are observed (fig.3a). But at higher concentration of BPQ, molecules are packed in two-dimensional fashion (sample D) to form crystalline hexagonal plate like geometry with equal thickness as shown in fig.3b. It seems a two dimensional growth of particles of length ~15-20μm and width ~8-10μm, take place with the increasing concentration of BPQ in solution. Most of the micro plates have smooth surface, suggesting that the luminogenic molecules (BPQ) are arranged uniformly within the crystals.

Optical microscopic study:

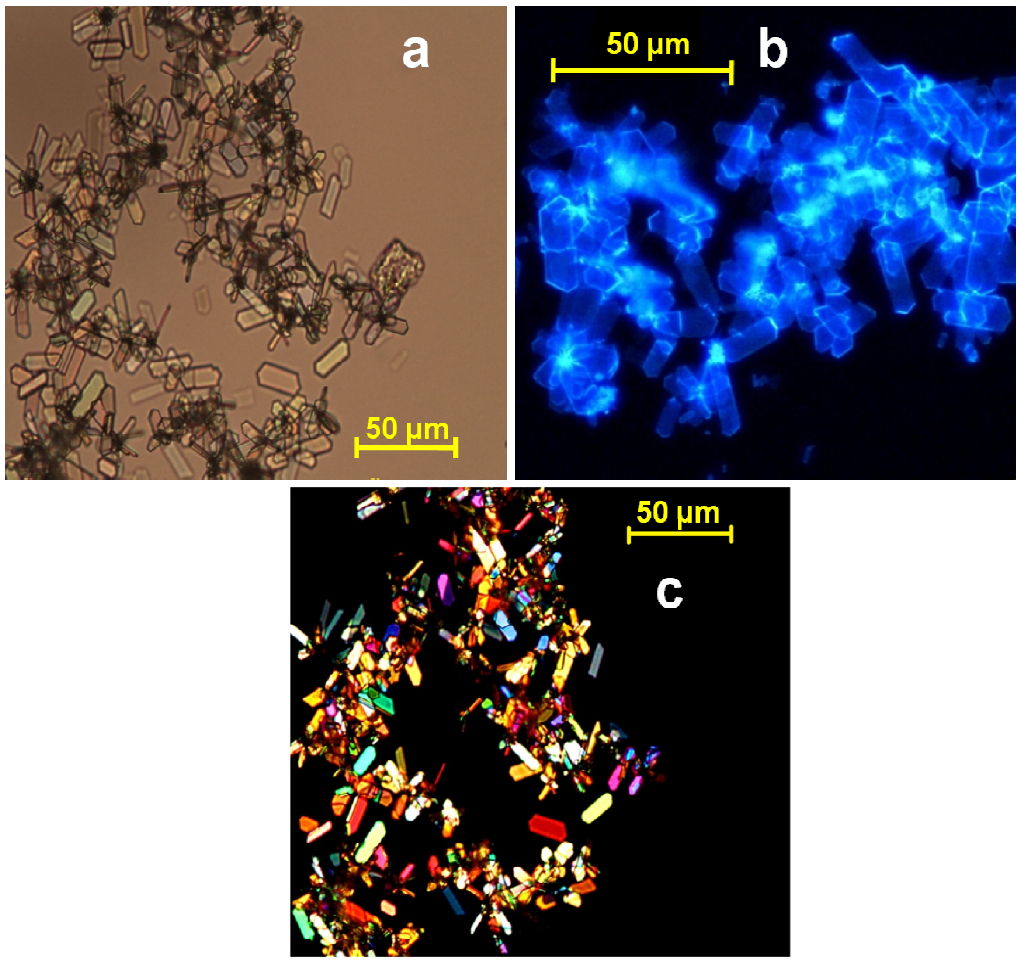

Fig.4 (a) Optical microscopic images of BPQ microcrystals have sample D (400µM BPQ), (b) Fluorescence microscopic images of BPQ microcrystals have sample D (400µM BPQ); exciting under UV light, (c) Polarized microscopic images of BPQ microcrystals having sample D (400µM BPQ).

Fig.4a shows the optical microscopic images of sample-D. The sizes of other samples (A, B and C) are too small to be detected within the resolution of our optical microscope. The morphology of the aggregated crystals of sample-D is hexagonal plate like and a clear two dimensional growth of crystals are noticeable. Fluorescence microscopic image of the crystals under UV excitation is shown in fig.4b. The micro plates are highly luminescent, emitting intense blue light upon UV excitation. This color resembles to the color of aggregates shown in the inset of fig.2b and it suggests that the nonemissive BPQ molecule

becomes blue emitter in its aggregated state. Dark field's view of sample D using polarizer, analyzer assembly shows different colors depending on the direction of incident radiation and it reveals the anisotropic nature of the synthesized microcrystal (Fig.4c).

pH dependent photophysical properties: The hydroxonium ion is one of the most important charged species that plays an important role in biological processes occurring in living cells and tissues such as proliferation and apoptosis, multidrug resistance, ion transport, endocytosis and muscle contraction. An interesting feature of the present compound is its pronounced effect of photophysical behavior upon protonation (Scheme 3).

Scheme 3: The proposed mechanism of BPQ for sensing H^+

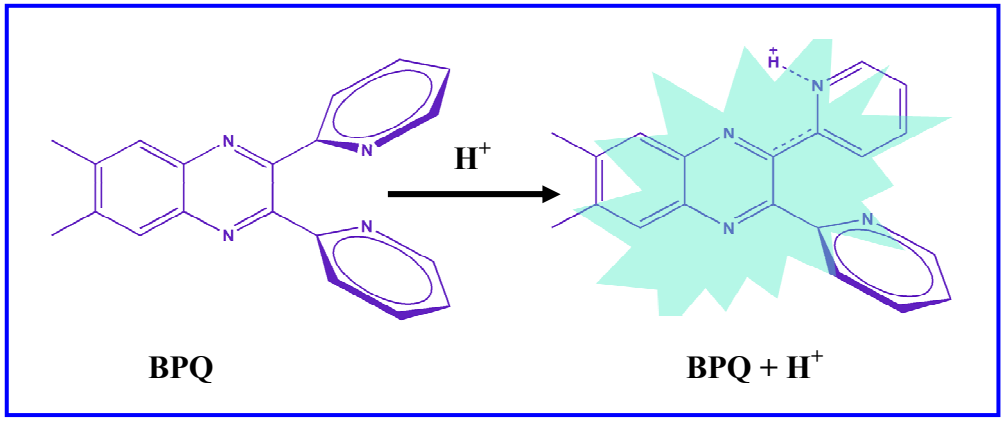

Absorption spectra of BPQ at different pH: The UV-Vis absorption spectra of BPQ hydrosol recorded at different pH values are shown in fig.5a. Protonated form of BPQ in the acidic pH shows broad absorption with absorption maxima at 361 nm. Absorption maxima of the deprotonated forms in the basic pH (>7) medium is at 354 nm. At higher pH (>7) absorption spectrum is similar to that of aggregated hydrosol in water. The spectra measured at higher pH are basically the same that of pH~5. The broadening and red shift of the emission spectra at pH<5 suggest the enhancement of charge transfer character in this molecule upon protonation.[56]

Fluorescence spectra of BPQ at different pH: Photoluminescence (PL) spectra of BPQ hydrosol at different pH are shown in Fig.5b. No change in PL spectra of the hydrosol is observed at pH≥5. But at pH less than 5, a new red shifted broad emission band having maxima at 468 nm is appeared. An isoemissive point between peak maxima 398 nm and 468 nm is observed and it indicates equilibrium between protonated and deprotonated species of BPQ. It is also observed that the milky hydrosol slowly turned into clear solution with increasing H^+ concentration in the medium. We presume that the broad emission band at 468 nm is due to the charge transfer emission from the dissolved protonated $BPQH^+$ in the solution. Addition of less polar THF to this acidic hydrosol (fig.5d) shows blue shift and decreasing intensity of the 468 nm broad band and hence it confirms the charge transfer character of the band.

A visual change in color (fig.5c) from blue to green under UV light excitation at higher (pH>4, blue) and lower pH (pH<4, green) is observed indicating the presence of mostly charge transfer protonated BPQ in the acidic solution. It is further observed that the intensity of 468 nm band decreases at higher H^+ ion concentrations (pH<1). It seems at higher H^+ ion concentrations, the nitrogen centre of quinoxaline unit get protonated and hence the charge transfer character of the molecule as a whole decreases.

We also investigated the reversibility of protonation/deprotonation processes of BPQ in its hydrosol. It is observed that the switch between blue and green emission can be repeated without fatigue by alternate addition of NaOH and HCl and the process is nondestructive in nature (fig.6a). The red shift of ~70 nm in the fluorescence of BPQ when being introduced with HCl and the recovery toward the initial blue emission (λ_{em} = 398 nm) demonstrate the significant fluorescent switching properties of the BPQ hydrosol under protonation/deprotonation stimuli (fig.6b).

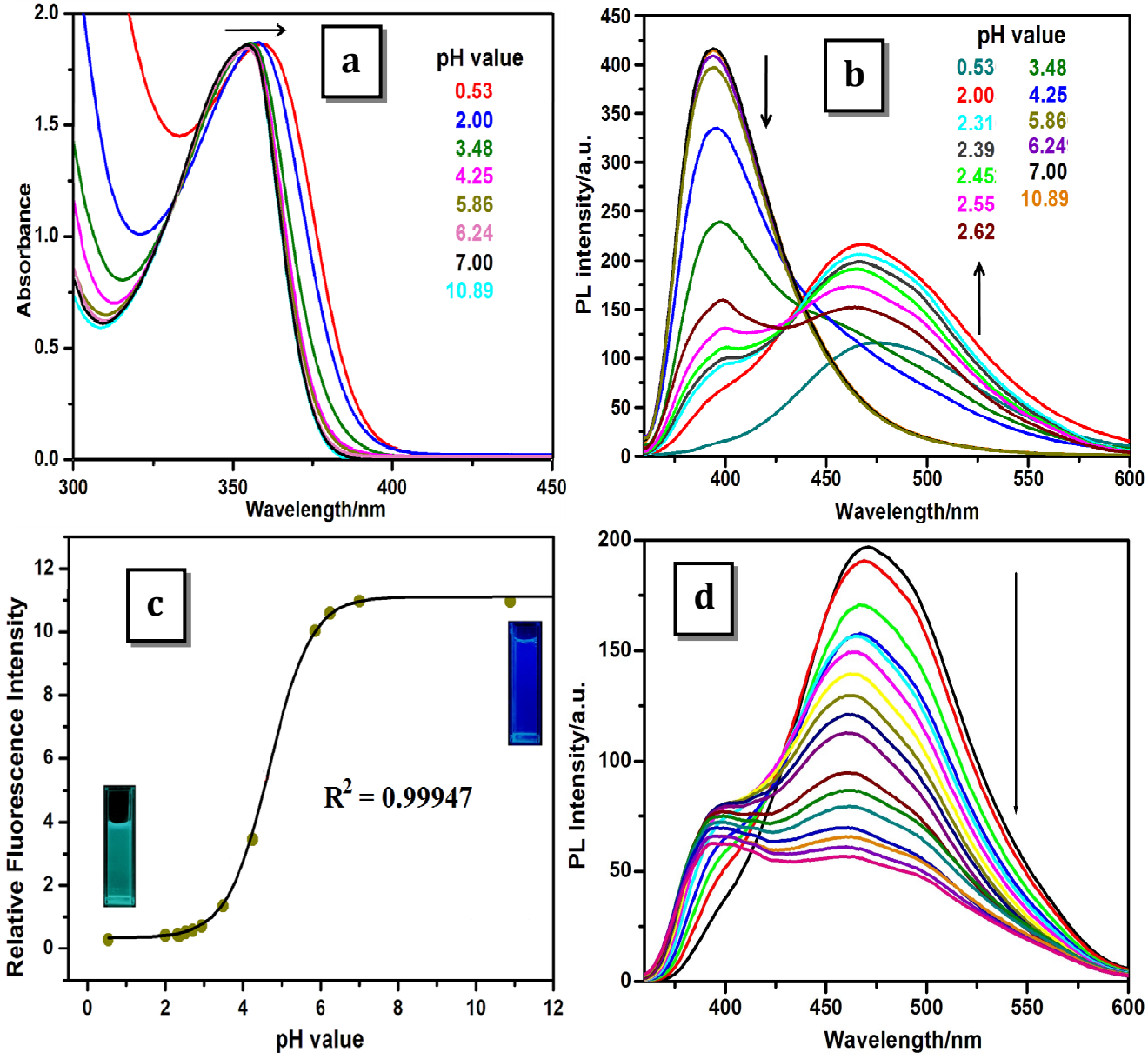

Fig.5 (a) Normalized UV-Vis absorption spectra of BPQ hydrosol (80μM) in THF/water mixture (10:90 v/v) at different pH of the medium (pH ~ 1.0-11.0). (b) PL spectra of BPQ hydrosol (80μM) in THF/water mixture (10:90 v/v) at different pH of the medium (pH ~ 1.0-11.0). λ_{ex}: 350 nm. (c) Ratiometric calibration curve of I_{398}/I_{468} (intensity at 398 nm vs. intensity at 468 nm as a function of pH of the medium and pH dependent color shift from green to blue with decreasing concentration of H^+ ion in the medium under 367 nm illumination. (d) PL spectra of protonated BPQ in water/THF mixture. λ_{ex}: 350 nm.

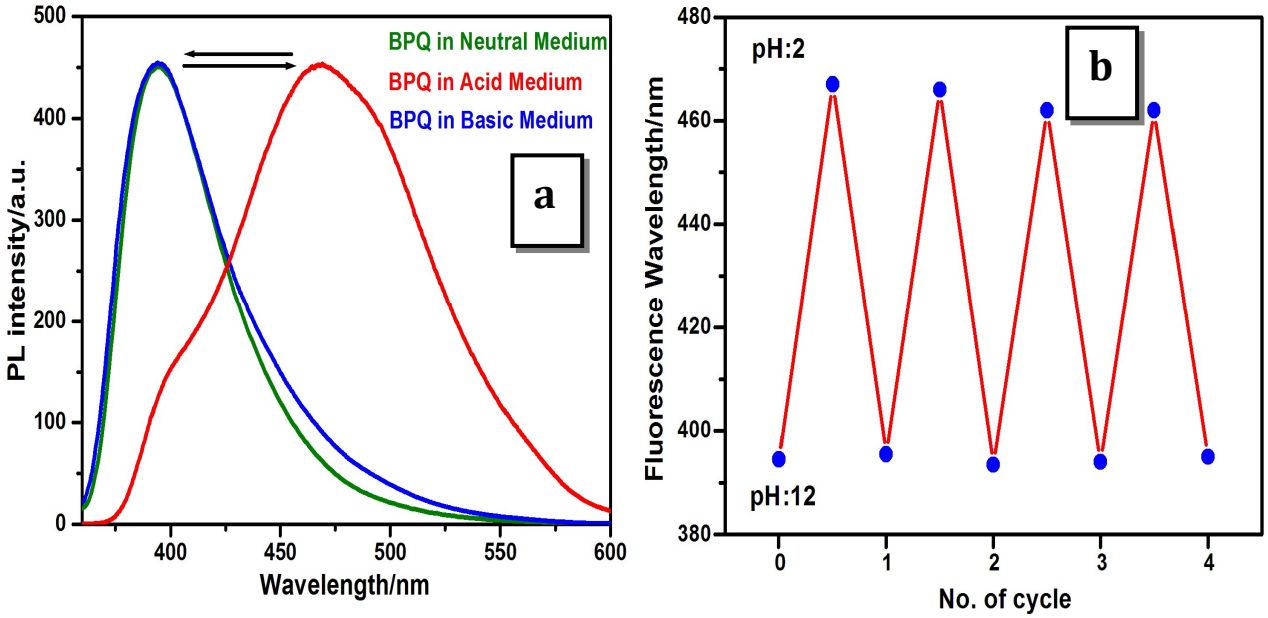

Fig.6 (a) Normalized PL spectra of aggregated BPQ by changing pH of the medium by acidic and basic solvent. (b) Reversible switching of the emission wavelength of BPQ by repeated adding of acid and alkali to the medium.

Time resolved Fluorescence Study: In order to understand the nature of aggregate of BPQ luminogen, we have carried out time resolved fluorescence study of aggregated BPQ hydrosols with excitation at 376 nm and emissions are measured at 398 nm and 468 nm for deprotonated and protonated BPQ hydrosols respectively. Decay profile of deprotonated and protonated hydrosols of BPQ are shown in fig.7a. Fluorescence lifetime of diluted BPQ in THF is difficult to measure due to very week emission intensity of the monomer. Fluorescence lifetimes of BPQ hydrosols are measured by deconvoluting the response function from the decay curves. The decay profiles of aggregated BPQ hydrosols having reasonably higher emission intensity are fitted with bi-exponential decay. The observed components of lifetime for aggregated BPQ lie within ~0.2ns and ~0.8-1.0ns respectively.

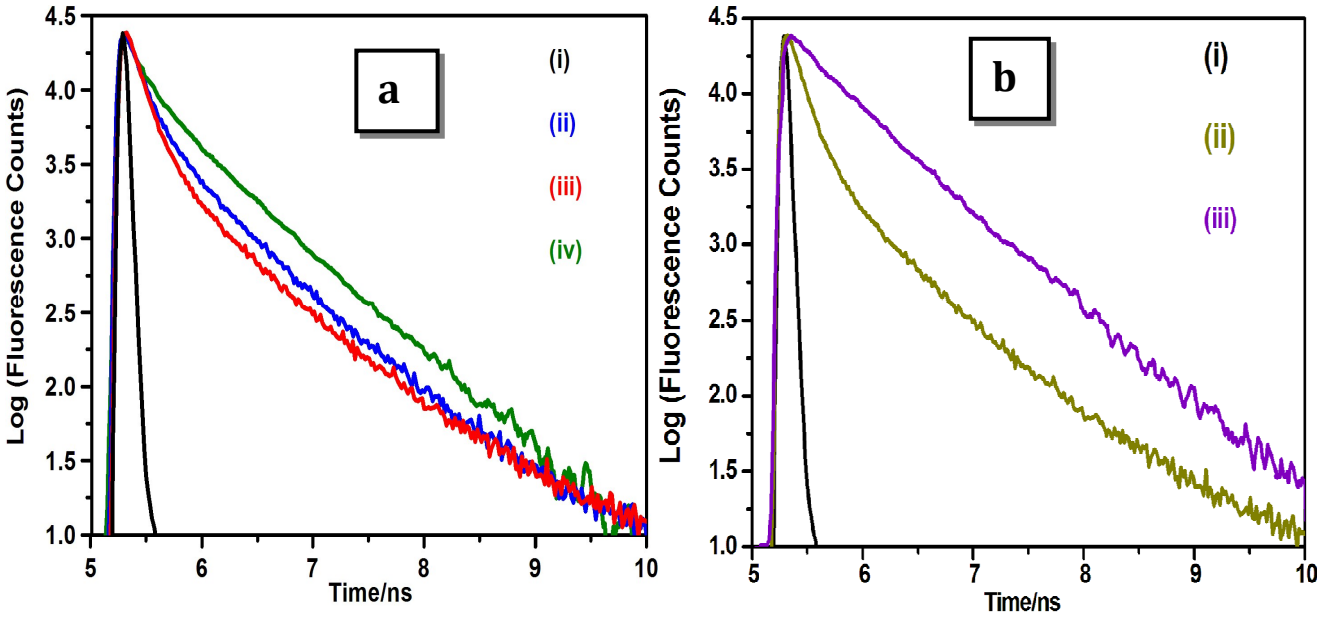

Fig.7 Fluorescence decay profile of spectra (a) (i) Lamp, (ii) sample A (40µM BPQ), (iii) sample B (80µM BPQ) and (iv) sample B (80µM BPQ) in pH~2 medium at (λ_{emi}: 398 nm). (b) (i) Lamp, (ii) sample B (80µM BPQ) at (λ_{emi}: 398 nm), (iii) sample B (80µM BPQ) in pH~2 medium at (λ_{emi}: 468 nm). Excitation wavelength: 376 nm.

The weight percentage of shorter component (~0.2ns) increases and the longer component (~1.0ns) decreases with the increasing size of the aggregates. BPQ molecules present within the aggregates are facing two types of micro environments *i.e.* surface bound BPQ and BPQ within the inner core of the microcrystals. The excited inner core BPQ molecules behave like Frenkel excitons whose fluorescence lifetime (~0.2ns) is much shorter than the surface bound molecules. Now with increasing size of the aggregates, the number of surface bound BPQ decreases and hence the weight percentage of the longer component decreases. On the other hand, with decreasing pH (<4) of the medium, dissolution of BPQ from aggregate to solution takes place and hence the size of the aggregate decreases. The number of surface bound BPQ increases with decreasing size of aggregates and it is reflected in the increasing weight percentage of the fluorescence lifetime of the surface bound molecules *i.e.*~1.0ns component (table-1). The competition between ICT and AIEE character at much higher proton concentration generate

a new peak at longer wavelength (468 nm). Interestingly the lifetime of protonated BPQ at this peak is fitted with single exponential decay and the value is ~0.8ns. This 0.8ns component arises solely from the solvated $BPQH^+$ upon excitation to its ICT state (fig.7b).

Table1: Fluorescence lifetime of aggregated hydrosols of 6,7-dimethyl-2,3-bis-(2-pyridyl)-quinoxaline (BPQ) in water (sample A and sample B) and sample B in pH~ 2.

Sample	τ_1 (ns)	Contribution (%)	τ_2 (ns)	Contribution (%)	χ^2
Sample A (λ_{emi}: 398 nm)	0.187	79.9	0.963	20.1	0.94
Sample B (λ_{emi}: 398 nm)	0.188	88.6	1.063	11.4	0.99
Sample B in pH~2 (λ_{emi}: 398 nm)	0.163	38.6	0.834	61.4	0.96
Sample B in pH~2 (λ_{emi}: 468 nm)			0.846	100	0.92

Mechanism of proton triggered tuning AIEE and ICT effect of BPQ: It was well documented that the spatial conformation of molecules played an important role in determining their stacking modes and thus influenced the properties of the resulting aggregate. In BPQ molecule, two pyridyl units are attached to the 2, 3 positions of 6, 7-dimethyl quinoxaline moiety through single bond. The coplanar arrangement of these two rings with quinoxaline groups are avoided due to steric forces and the BPQ as a whole prefer to attain a twisted geometry. Optimized ground state geometry of BPQ using DFT/B3LYP/6-31G(d,p) level of theory shows that both the pyridyl unit prefer to remain ~140^0 out of plane of the quinoxaline ring. The twisted pyridyl ring will increase the stacking distance between two immediate neighbors at about ~ 5Å within the aggregates and it results much weaker intermolecular π-π stacking interaction. The free rotation of two pyridyl groups is also hindered in the aggregated state to make the molecule AIEE active. But a significant conformational change of BPQ is observed in acidic medium. The frontier molecular orbital (FMO) of BPQ and $BPQH^+$ calculated using DFT/B3LYP/6-

31G(d,p) level of theory are shown in fig.8. HOMO electron densities of BPQ are localized within the quinoxaline and pyridyl moiety separately and the electron densities are shifted from donor pyridyl to acceptor quinoxaline moiety in its LUMO. This delocalization of excited electronic energy with the freely rotating pyridyl group is responsible to open up the non-radiative deactivation channels for excited BPQ in its isolated form in solution and allow the charge transfer from donor pyridyl group to acceptor quinoxaline group. On the other hand though electron density on the protonated pyridyl group is absent in HOMO of $BPQH^+$, the electron density is shifted to pyridyl group in its LUMO. This drift of electron density from quinoxaline group to pyridyl group in the excited state is due to the formation of strongly electron-withdrawing pyridinium ion, which triggered the intramolecular charge transfer between the quinoxaline donor and the pyridinium acceptor.

In acidic medium, the proton (H^+) will first attached with nitrogen atom of the pyridyl groups since the pK_a value of pyridyl unit (5.25) is much higher than that of quinoxaline (0.6). Through aromatic conjugation, the quinoxaline loses electron density while the pyridinium ion gains electron density. Thus a prominent intramolecular charge transfer character from donor quinoxaline to acceptor protonated pyridyl group takes place and it is reflected in the lowering of HOMO and LUMO energy gap after protonation from 4.33eV to 3.15eV as shown in fig.8. This aromatic conjugation stabilizes the LUMO mostly and causes red-shift of both the absorption and emission spectra of $BPQH^+$ (fig.5a and 5b).

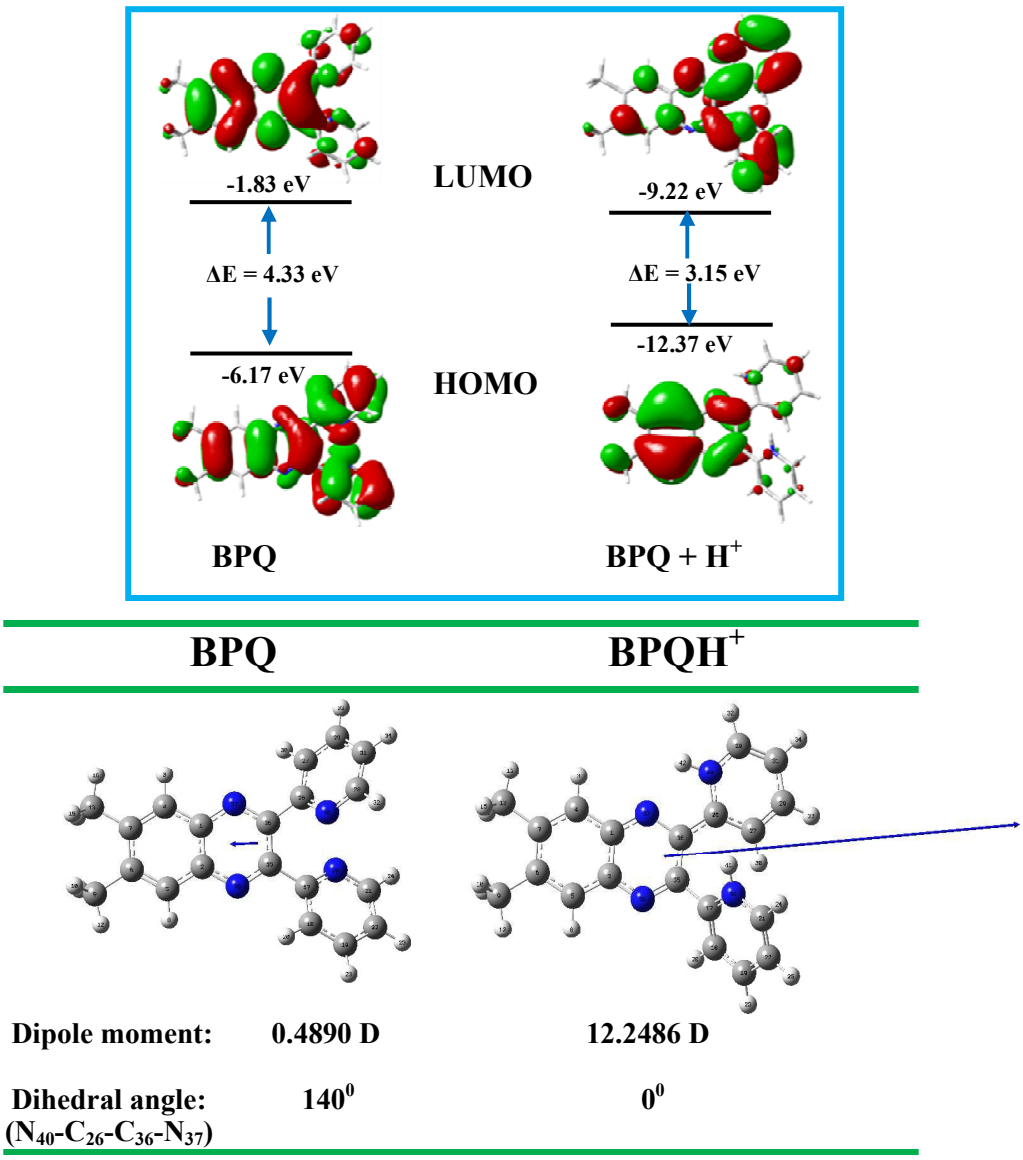

Fig.8 Theoretically calculated frontier orbital of BPQ and $BPQH^+$ calculated by using the DFT B3LYP/6-31G(d,p) basis set. The optimized geometry, dipole moment and dihedral angle between two nitrogen of pyridyl and quinoxaline moiety of BPQ and $BPQH^+$ molecule at its lowest excited state (S_1) calculated by using the TDDFT B3LYP/6-31G(d,p) basis set.

Introduction of ICT character in protonated BPQ is further supported from the excited state optimized geometry of both protonated and deprotonated BPQ molecule (fig.8). BPQ molecule is in twisted geometry, both in ground and excited state and the twisted angle between quinoxaline and pyridyl

group is ~140^0. But after protonation at pyridyl centre, planarity (N_{40}-C_{26}-C_{36}-N_{37} ~ 10^0) is introduced in one of the protonated pyridyl group in the ground state and dihedral angle N_{40}-C_{26}-C_{36}-N_{37} decreases to zero in the excited state. Meanwhile, it induces the dipole moments in the reversed directions (fig.8). An enhanced value of dipole moment from 0.489 D to 12.2486 D is also observed after protonation. This enhancement of dipole moment supports the introduction of polarity and at the same time ICT character in $BPQH^+$.

4. Picric Acid Sensor:

UV-Vis spectra of BPQ hydrosol in presence of picric acid generate a new peak at longer wavelength region *i.e.* at 400 nm (fig.9a). The broad red shifted band at 400 nm gradually becomes prominent with the increase of picric acid concentration to a fixed amount of BPQ hydrosol. Being a strong electron deficient molecule, PA can easily be attracted towards electron rich aggregated BPQ to form non fluorescent ground state complex and the red shifted (400 nm) band is the charge transfer band.[55] But the addition of other nitroaromatic compounds to BPQ hydrosol does not show any change in the absorption spectrum because their electron deficiency cannot reach to such extent to form strong complex with fluorescent BPQ hydrosol.

The fluorescence spectrum of BPQ hydrosol exhibits an intense emission peak at 398 nm. This fluorescence is effectively quenched upon addition of PA. Fig. 9b shows the changes in the fluorescence spectrum upon titration of the hydrosol against picric acid solution. Gradual addition of PA to BPQ hydrosol, the emission intensity decreases, but the PL spectra profile remains unchanged. The plot of I_0/I versus [PA] shows an upward curvature instead of linear relationship (inset of fig.9c), indicating that quenching efficiency increases with increasing concentration of quencher and may be termed as super amplified quenching effect.[57-60] The unique phenomenon could be attributed to the 3-dimensional morphology of the aggregates that generate more small cavities to enable the small explosive molecules

to enter through electrostatic interactions and offer more diffusion channels for the excitons to migrate, allowing them to be more quickly annihilated by the explosive quenchers.

Equation $I_0/I = 1.146 + 0.329e^{0.14684[PA]}$ is obtained by fitting the concave curve of fig.9c. From this equation, quantitative analysis can be realized. But the curvature nature of this Stern-Volmer plot may be due to either static or dynamic pathway. This ambiguity is resolved by measuring fluorescence lifetime of BPQ hydrosol in presence and absence of PA (inset of fig.9b).[61,62] Our measured fluorescent decay curves of BPQ hydrosol both in presence and absence of PA are fitted with bi-exponential decay and the fitted components are identical for both the cases(inset of fig.9b). This unchanged fluorescence lifetime of BPQ hydrosol in the presence of PA indicates that the fluorescence quenching takes place through ground state complexation *i.e.* static quenching mechanism. At low concentration of PA (inset of fig.9c) a linear Stern-Volmer plot is obtained with quenching constant value 7.81×10^4 M^{-1}. Fluorescence quenching of BPQ in presence of different aromatic nitro compounds (3-NBA, 3,5-DNBA, NA, DNB, DNT, NP, DNP, PA) are also studied (fig.9d) and it is observed that the quenching efficiency of PA is much higher than other nitro aromatics. The lowest detection limit of PA was calculated using 3σ method and the value is 0.77μM.[63]

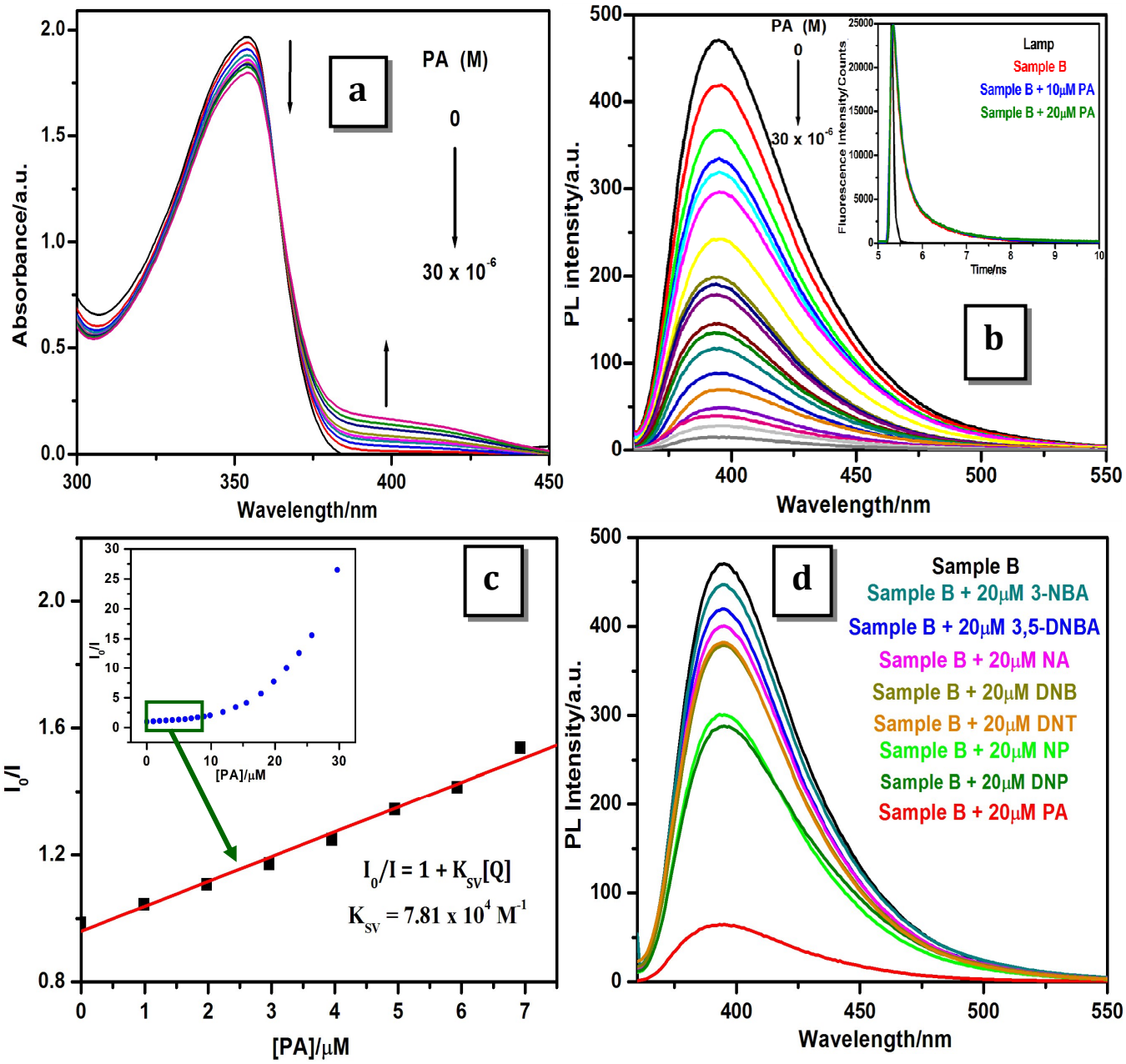

Fig.9 (a) UV-Vis spectra and (b) Fluorescence spectra of BPQ hydrosol (80μM BPQ) after the addition of different amounts of PA. The inset shows the variation of fluorescence lifetime of BPQ hydrosol (80μM BPQ) in absence and presence of PA (10 and 20μM) at (λ_{emi}: 398 nm). Excitation wavelength: 376 nm. (c) Stern-Volmer curve of corresponding fluorescence quenching in presence of different amount of PA. The inset shows a plot of I_0/I versus [PA] for BPQ hydrosol. (d) Comparison of fluorescence quenching of BPQ hydrosol in presence of different aromatic nitro compounds (20μM).

5. Conclusion:

In conclusion, we have introduced a low dimensional aggregated hydrosol from the pyridyl substituted quinoxaline (BPQ) that possesses remarkable AIEE properties. Aggregation has induced significant enhancements in its fluorescence efficiency compared with its dilute solution in good solvent. The behavior has been explained due to restriction of intramolecular rotation and large amplitude vibrational modes in its aggregated states. In addition, we have presented the proton-triggered red shifted luminescence of BPQ hydrosol. Computation of HOMO, LUMO electron densities of BPQ and $BPQH^+$ reveals extended conjugation of electron density between quinoxaline and pyridyl group takes place upon photoexcitation of $BPQH^+$. This ICT in $BPQH^+$ causes the switching of emission from blue to green in presence of excess H^+ ions. Thus, introduction of an AIEE unit to the traditional pH sensitive fluorophores is an efficient route to expand their practical application to both solution and solid states. Such results also provide valuable information on the future design of new fluorescent probes, whose light-emitting behavior can be readily tuned by simply varying the environmental conditions. Another excellent utility of this AIEE active molecule is its selective sensitivity towards picric acid (PA) with quenching constant 7.81×10^4 M^{-1}. It is further explained with the help of both steady state and time resolved emission study that the fluorescence quenching of BPQ hydrosol in presence of picric acid takes place through static quenching mechanism.

Keywords: Aggregation induced emission enhancement, Intramolecular charge transfer, pH, bathochromic shift, DFT, BPQ, Picric acid sensor.

Author information:

Corresponding Author:

E-mail: ajay@mail.vidyasagar.ac.in and ajaymsr@yahoo.co.in;

Fax: +91 3222 275329

Acknowledgement:

We gratefully acknowledge the financial support received from CSIR (Ref. No. 01(2443)/10/EMR-II), New Delhi for carrying out this research work. P.M., S.M. thank CSIR, New Delhi and M.S. thanks RGNF for their research fellowship. We thank to UGC, New Delhi for financial assistance through UGC innovative research program of Vidyasagar University. We acknowledge the help render by USIC, Vidyasagar University for doing fluorescence and optical microscopic measurements. We are also thankful to nano centre, Calcutta University, Kolkata and IIT KGP for doing FESEM and time resolved fluorescence study.

Reference:

1. S. Lee, K. K. Y. Yuen, K. A. Jolliffe and J. Yoon, *Chem. Soc. Rev.*, 2015, **44**, 1749-1762.

2. H. N. Kim, Z. Guo, W. Zhu, J. Yoon and H. Tian, *Chem. Soc. Rev.,* 2011*,* **40***,* 79-93.

3. D. W. Domaille, E. L. Que and C. J. Chang, *Nat. Chem. Biol.,* 2008, **4,** 168-175.

4. Z. Xu, J. Yoon and D. R. Spring, *Chem. Soc. Rev.,* 2010, **39**, 1996-2006.

5. W. P. Ambrose, P. M. Goodwin, J. H. Jett, A. V. Orden, J. H. Werner and R. A. Keller, *Chem. Rev.* 1999, **99,** 2929.

6. W. F. Patton, *Biotechniques,* 2000, **28,** 944.

7. Y. Gong, J. Liu, Y. Zhang, G. He, Y. Lu, W. B. Fan, W. Z. Yuan, J. Z. Sun and Y. Zhang, *J. Mater. Chem. C*, 2014, **2**, 7552-7560.

8. J. Huang , N. Sun , J. Yang , R. Tang , Q. Li, D. Ma, J. Qin and Z. Li, *J. Mater. Chem.,* 2012, **22,** 12001-12007.

9. J. Li, F. Yan, J. Gao, P. Li, W.W. Xiong, Y. Zhao, X. W. Sun and Q. Zhang, *Dyes and Pigments,* 2015, **112,** 93-98.

10. S. C. Price, A. C. Stuart, L. Yang, H. Zhou and W. You, *J. Am. Chem. Soc.,* 2011, **133,** 4625- 4631.

11. A. J. Heeger, *Chem. Soc Rev.* 2010, **39,** 2354-2371.

12. X. Guo, R. P. Ortiz, Y. Zheng, M. G. Kim, S. Zhang, Y. Hu, G. Lu, A. Facchetti and T. J. Marks*, J.*

Am. Chem. Soc. 2011, **133,** 13685-13697.

13. M. M. Durban, P. D. Kazarinoff, Y. Segawa and C. K. Luscombe, *Macromolecules,* 2011, **44,** 4721-4728.
14. Y. Hong, J. W. Y. Lam and B. Z. Tang, *Chem. Commun.,* 2009, 4332-4353.
15. P. Mazumdar, D. Das, G. P. Sahoo, G. S. Morán and A. Misra, *Phys. Chem. Chem. Phys.,* 2014, **16** 6283-6293.
16. M. Wang, D. Zhang, G. Zhang and D. Zhu, *Chem. Commun,* 2008, 4469-4471.
17. P. Mazumdar, D. Das, G. P. Sahoo, G. S. Morán and A. Misra, *Phys. Chem. Chem. Phys.,* 2015, **17** 3343-3354.
18. D. Das, G. P. Sahoo, P. Mazumdar, A. Maity, D. Chattopadhyay, G. S. Morán and A. Misra, *J. Mol. Liq.,*2015, **206,** 47-55.
19. G. P. Sahoo, D. Das, P. S. Sheet, H. Beg, G. S. Morán and A. Misra, *RSC Adv.,* 2014, **4** 10903-10911.
20. J. Luo, Z. Xie, J. W. Y. Lam, L. Cheng, H. Chen, C. Qiu, H. S. Kwok, X. Zhan, Y. Liu, D. Zhu and B. Z. Tang, *Chem. Commun.* 2001, 1740-1741.
21. B.K. An, S.K. Kwon, S.D. Jung and S. Y. Park, *J. Am. Chem. Soc.,* 2002, **124,** 14410-14415.
22. Y. Hong, J. W. Y. Lam and B. Z. Tang, *Chem. Soc. Rev.,* 2011, **40,** 5361-5388.
23. R. Wei, P. Song and A. Tong, *J. Phys. Chem. C,* 2013, **117**, 3467-3474.
24. W. Liu, Y. Wang, M. Sun, D. Zhang, M. Zheng and W. Yang, *Chem. Commun.* 2013, **49**, 6042-6044.
25. Z. Chang, Y. Jiang, B. He, J. Chen, Z. Yang, P. Lu, H. S. Kwok, Z. Zhao, H. Qiu and B. Z.Tang, *Chem.Commun*., 2013, **49**, 594-596.
26. R. Hu, S. Li, Y. Zeng, J. Chen, S. Wang, Y. L. and G. Yang, *Phys. Chem. Chem. Phys.,* 2011,**13**, 2044-2051.
27. Z. Zheng, Z. Yu, M. Yang, F. Jin, Q. Zhang, H. Zhou, J. Wu and Y. Tian, *J. Org. Chem.,* 2013, **78**, 3222-3234.

28. J. Liu, Q. Meng, X. Zhang, X. Lu, P. He, L. Jiang, H. Dong and W. Hu, *Chem.Commun,* 2013, **49**, 1199-1201.

29. Q. Li and L. Blancafort, *Chem. Commun,* 2013, **49**, 5966-5968

30. Z. Zhao, S. Chen, J. W. Y. Lam, Z. Wang, P. Lu, F. Mahtab, H. H. Y. Sung, I. D. Williams, Y. Ma, H.S. Kwok and B.Z.Tang, *J. Mater. Chem.,* 2011, **21**, 7210-7216.

31. H. Li, Z. Chi, B. Xu, X. Zhang, X. Li, S. Liu, Y. Zhang and J.Xu, *J. Mater. Chem.*, 2011, **21**, 3760-3767.

32. E. L. Spitler and M. M. Haley, *Tetrahedron,* 2008, **64,** 11469-11474.

33. D. Knapton, S. J. Rowan and C. Weder, *Macromolecules,* 2006, **39,** 651-657.

34. P. K. Iyer, J. B. Beck, C. Weder and S. J. Rowan, *Chem. Commun.,* 2005, 319-321.

35. J. J. Lavigne and E. V. Anslyn, *Angew. Chem., Int. Ed.,* 1999, **38,** 3666-3669.

36. C. Dou, L. Han, S. Zhao, H. Zhang and Y. Wang, *J. Phys. Chem. Lett.*, 2011, **2,** 666-670.

37. E. A. Davey, A. J. Zucchero, O. Trapp and U. H. F. Bunz, *J. Am. Chem. Soc.* 2011, **133,** 7716-7718.

38. A. J. Zucchero, J. N. Wilson and U. H. F. Bunz, *J. Am. Chem. Soc.* 2006, **128,** 11872-11881.

39. Z. Yang, W. Qin, J. W. Y. Lam, S. Chen, H. H. Y. Sung, I. D. Williams and B. Z. Tang, *Chem. Sci.* 2013, **4**, 3725-3730.

40. J. Tolosa, K. M. Solntsev, L. M. Tolbert and U. H. F. Bunz, *J. Org. Chem.* 2010, **75,** 523-534.

41. S. Ma, J. Zhang, J. Chen, L. Wang, B. Xu and W. Tian, *Chin. J. Chem.* 2013, **31,** 1418-1422.

42. J. Chen, S. Ma, J. Zhang, L. Wang, L. Ye, B. Li, B. Xu and W. Tian, *J. Phys. Chem. Lett*. 2014, **5,** 2781-2784.

43. R. Murugavel and M. P. Singh, *New J. Chem.,* 2010, **34**, 1846-1854.

44. B. Szczesna and Z. U. Lipkowska, *New J. Chem.,* 2002, **26,** 243-249.

45. P. K. Thallapally, A. K. Katz, H. L. Carrell and G. R. Desiraju, *Chem. Commun.,* 2002, 344-345.

46. K. K. Kartha, A. Sandeep, V. K. Praveen and A. Ajayaghosh, *Chem. Rec.*, 2015, **15**, 252-265.

47. N. Niamnont, N. Kimpitak, K.Wongravee, P. Rashatasakhon, K. K. Baldridge, J. S. Siegel and M.

Sukwattanasinitt, *Chem. Commun*., 2013, **49**, 780-782.

48. N. Dey, S. K. Samanta and S. Bhattacharya, *ACS Appl. Mater. Interfaces,* 2013, **5**, 8394-8400.

49. V. Bhalla, A. Gupta, M. Kumar, D. S. S. Rao and S. K. Prasad, *ACS Appl. Mater. Interfaces, 2013, **5**,* 672-679.

50. M. Kumar, S. I. Reja and V. Bhalla, *Org. Lett*., 2012, **14**, 6084-6087.

51. R. Ni, R. B. Tong, C. C. Guo, G. L. Shen and R. Q. Yu, *Talanta,* 2004, **63**, 251-257.

52. V. Bhalla, A. Gupta and M. Kumar, *Org. Lett.* 2012, **14**, 3112-3115.

53. P. R. Bevington, McGraw Hill, *New York,* 1969, 235-237.

54. FELIX 32, *Operation Manual, Version 1.1, Photon Technology International*, Inc., Birmingham, NJ, 2003.

55. K. K. Kartha, V. K. Praveen, S. S. Babu, S. Cherumukkil and A. Ajayaghosh, *Chem. Asian J.*, 2015, **10**, 2250-2256.

56. S. Shanmugaraju, D. Samanta, B. Gole and P. S. Mukherjee, *Dalton Trans.*, 2011, **40**, 12333-12341.

57. W. Wei, R. Lu, S. Tang and X. Liu, *J. Mater. Chem. A,* 2015, **3**, 4604-4611.

58. K. Acharyya and P. S. Mukherjee, *Chem. Commun.,* 2014, **50**, 15788-15791.

59. S. Sanda, S. Parshamoni, S. Biswas and S. Konar, *Chem. Commun.,* 2015, **51**, 6576-6579.

60. J. Wang, J. Mei, W. Yuan, P. Lu, A. Qin, J. Sun, Y. Mac and B. Z. Tang, *J. Mater. Chem.,* 2011, **21**, 4056-4059.

61. P. Lu, J. W. Lam, J. Z. Liu, C. K. Jim, W. Z. Yuan, N. Xie, Y. C. Zhong, Q. Hu, K. S. Wong, K. K. Cheuk and B. Z. Tang, *Macromol. Rapid Commun.* 2010, **31**, 834-839.

62. X. Sun, Y. Wang and Y. Lei, *Chem. Soc. Rev*. 2015, **31**, DOI: 10.1039/c5cs00496a.

63. Y.B. Ruan, A.F. Li, J.S. Zhao, J.S. Shen and Y.B. Jiang, *Chem. Commun.,* 2010, **46**, 4938-4940.